Japanese Journal of Applied Physics

The Japan Society of Applied Physics

RAPID COMMUNICATION • OPEN ACCESS

Dry and wet etching for β-Ga_2O_3 Schottky barrier diodes with mesa termination

OPEN ACCESS

Japanese Journal of Applied Physics **58**, 120902 (2019) **RAPID COMMUNICATION**

https://doi.org/10.7567/1347-4065/ab4f90

Dry and wet etching for β-Ga_2O_3 Schottky barrier diodes with mesa termination

Hironori Okumura[1*] and Taketoshi Tanaka[2]

[1]*Faculty of Pure and Applied Science, University of Tsukuba, Tsukuba 305-8573, Japan*
[2]*Rohm Co. Ltd., Kyoto 615-8585, Japan*

*E-mail: okumura.hironori.gm@u.tsukuba.ac.jp

Received October 1, 2019; revised October 17, 2019; accepted October 21, 2019; published online November 6, 2019

We investigated dry and wet etchings of β-Ga_2O_3 and fabricated vertical Schottky barrier diodes (SBDs) with mesa termination using the optimal etching condition. Using an inductively-coupled plasma reactive-ion etching with a nickel-hard mask, a β-Ga_2O_3 (010) mesa structure with a smooth sidewall is obtained at an etching rate of 77 nm min^{-1} in BCl_3/Cl_2 mixture gas. By immersing β-Ga_2O_3 (001) vertical SBDs with mesa termination in hot phosphoric-acid solution, the specific on resistance and ideality factor of the SBDs are reduced to 0.91 mΩcm^2 and 1.03, respectively. Current density at reverse bias is in good agreement with thermionic field emission model.

Ga_2O_3 is one of the promising materials for high-power applications due to its high critical electric field of 8 MV cm^{-1} and a large band-gap energy above 4.5 eV.[1)] Bulk Ga_2O_3 with a β-gallia phase, which is the most thermally stable, is grown using melt-based methods,[2)] potentially providing scalable wafers at a low cost. Recently, β-Ga_2O_3 fin field-effect transistors and trench metal-oxide-semiconductor (MOS) diodes have shown an excellent performance of high breakdown voltages over 1 kV.[3–5)] Still, the specific on-resistance R_{on} is over 5 mΩcm^2 at 1 kV, which is much higher than the theoretical limits. These vertical devices use a deep etching to prevent the high electric field near the surface region, suffering from a plasma damage by an inductively-coupled plasma (ICP) reactive-ion etching (RIE).[6)] Single crystal Ga_2O_3 is etched by chlorine-based RIE.[7–9)] The plasma damage can substantially reduce a carrier mobility,[10)] increasing R_{on}. The high-power β-Ga_2O_3 devices with low R_{on} require less plasma damage.

The plasma damage can be efficiently removed by etching with a chemical reaction. In fact, β-Ga_2O_3 Schottky barrier diodes (SBDs) with nearly unity ideality factor n are achieved by immersing in hot phosphoric-acid (H_3PO_4) solution after ICP-RIE.[11)] A Ga_2O_3 single crystal poses an excellent chemical stability. β-Ga_2O_3 is slightly etched by heating in nitric acid (HNO_3), sulfuric acid (H_2SO_4), H_3PO_4, and potassium hydroxide (KOH) solutions. The etch rate of β-Ga_2O_3 (100) at 120 °C is 1.4 nm min^{-1} for HNO_3 (61 wt%),[12)] ~2 nm min^{-1} for H_2SO_4 (97 wt%),[13)] and ~10 nm min^{-1} for H_3PO_4 (85 wt%).[14)] In hot KOH solution, photo-enhanced chemical etching with ultraviolet illumination increases the etch rate to 30 nm min^{-1} for (010) plane and 150 nm min^{-1} for $(\bar{2}01)$ plane.[15)] The effect of these chemical solutions on Ga_2O_3 devices has not been compared. In this study, we etched β-Ga_2O_3 under various ICP-RIE conditions and chemical solutions, and investigated the effect of various chemical solutions on the vertical β-Ga_2O_3 SBDs with mesa termination.

For dry and wet etching, we used tin-doped β-Ga_2O_3 (010) substrates (Novel Crystal Technology, Inc.). The substrate surfaces were treated by chemical mechanical polishing (CMP). The tin concentration was 4×10^{18} cm^{-3}. After solvent cleaning with acetone and isopropanol, a 50-nm-thick nickel-metal mask was deposited on the substrate using an electron beam (EB) evaporation. The ridge structures with ~300-nm heights were formed using ICP-RIE (Samco RIE-400iPS) with BCl_3 and Cl_2 mixture gases. An etch rate of the Ga_2O_3 layers was determined by scanning electron microscopy (SEM). After removing the nickel-metal mask using piranha (H_2SO_4 (95 wt%): H_2O_2 (30–35wt%) = 3:1) for 1 min, the substrates were dipped in various chemical solutions without starring on a heater for 10–30 min to remove the plasma damage. As the chemical solutions, we used piranha, H_3PO_4 (85 wt%), hydrofluoric acid (HF, 46–48 wt%), tetramethylammonium hydroxide (TMAH, 2 wt%), and KOH (3 wt%). The solution temperature was monitored by thermocouple in the heater. The wet-etched surfaces were observed by SEM.

The etch-rate dependence of β-Ga_2O_3 (010) on the ratio of Cl_2 and BCl_3 gases using ICP-RIE is shown in Fig. 1(a). The ICP power, bias power, cooling-water temperature, and chamber pressure were 150 W, 30 W, 20 °C, and 0.6 Pa, respectively. For the BCl_3/Cl_2 mixture gas, the etch rate of Ga_2O_3 increased with increasing the BCl_3 gas composition, corresponding to the other report.[16)] This indicates that not only the chlorine radicals in the plasma, but also unsaturated radicals produced from the BCl_3 additive contribute to the Ga_2O_3 etching.[8,17,18)] As shown in Fig. 1(b), the etch rate of Ga_2O_3 increased with increasing the ICP power. The high ICP power increases the plasma density, or the number of chlorine radicals, enhancing the chemical reaction on surfaces. The chemical etching provides a lower plasma damage in comparison with sputtering. The etch rate of 97 nm min^{-1} was achieved at the ICP power of 400 W with the Cl_2/BCl_3 mixing gas of 10/10 sccm.

The bird-view SEM images of the Ga_2O_3-ridge structure after ICP-RIE are shown in Fig. 2. The Ga_2O_3-ridge structures etched with only BCl_3 gas had the rough sidewall, as shown in Fig. 2(a), while those etched with the BCl_3/Cl_2 mixture gas had the smooth sidewall, as shown in Fig. 2(b). We suppose that the nickel-metal mask reacts with oxide in Ga_2O_3 for the ICP-RIE with BCl_3 gas, causing the redeposition of Ni-O impurities around the sidewall. Photoresist and SiO_2 may be used as a mask for ICP-RIE using only BCl_3

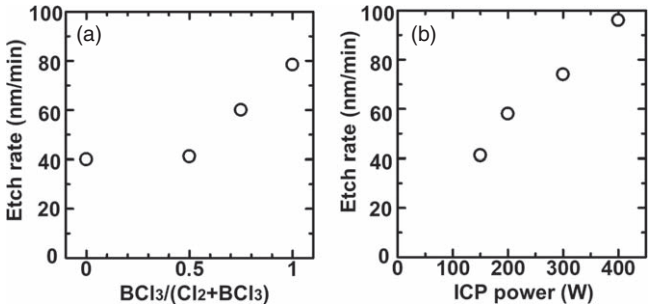

Fig. 1. (a) Etch-rate dependence of β-Ga_2O_3 (010) on ratio of Cl_2 and BCl_3 gases using ICP-RIE. ICP power, bias power, cooling-water temperature, and pressure were 150 W, 30 W, 20 °C, and 0.6 Pa, respectively. (b) Etch-rate dependence of β-Ga_2O_3 (010) on ICP power using ICP-RIE. BCl_3 gas flow, Cl_2 gas flow, bias power, cooling-water temperature, and pressure were 10 sccm, 10 sccm, 30 W, 20 °C, and 0.6 Pa, respectively.

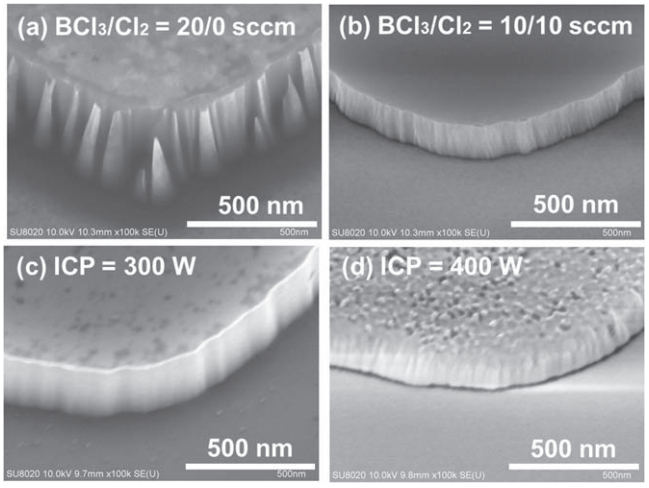

Fig. 2. Bird-view SEM image of β-Ga_2O_3 (010) etched by ICP-RIE; (a) BCl_3 gas flow of 20 sccm and ICP power of 150 W, (b) BCl_3 gas flow of 10 sccm, Cl_2 gas flow of 10 sccm, and ICP power of 150 W, (c) BCl_3 gas flow of 10 sccm, Cl_2 gas flow of 10 sccm, and ICP power of 300 W, and (d) BCl_3 gas flow of 10 sccm, Cl_2 gas flow of 10 sccm, and ICP power of 400 W. For all samples, bias power, cooling-water temperature, and pressure were 30 W, 20 °C, and 0.6 Pa, respectively.

gas. The roughness of the sidewall was independent on the ICP power, as shown in Fig. 2(c). The 50-nm-thick nickel mask was removed for 3 min at the ICP power of 400 W, as shown in Fig. 2(d), indicating the selectivity of ∼6, which is higher than the SiN_x mask.[18)]

After etching β-Ga_2O_3 (010) at the ICP power of 300 W with the Cl_2/BCl_3 mixture gas of 10/10 sccm and removing the nickel mask, the Ga_2O_3-ridge structures were dipped in various acid and alkali solutions. Although both solutions of HF at room temperature and piranha at 120 °C hardly etch β-Ga_2O_3 (010), the H_3PO_4 solution at 80 °C shows slightly anisotropic etching, as shown in Fig. 3(b). These solution temperatures were too small precisely to determinate the etch rate. Zhang et al. reported that hot H_3PO_4 solution of β-Ga_2O_3 (010) has a higher etch rate of the vertical plane to near [101] and [001] directions than that of the vertical plane to near [−101] and [103] directions.[14)] The appeared plane in hot H_3PO_4 solution may be the stable plane, or the vertical plane to near [−101] and [103] directions.

The TMAH solutions hardly etch β-Ga_2O_3 (010) at 80 °C, as shown in Fig. 3(c), while the KOH solutions at 80 °C show

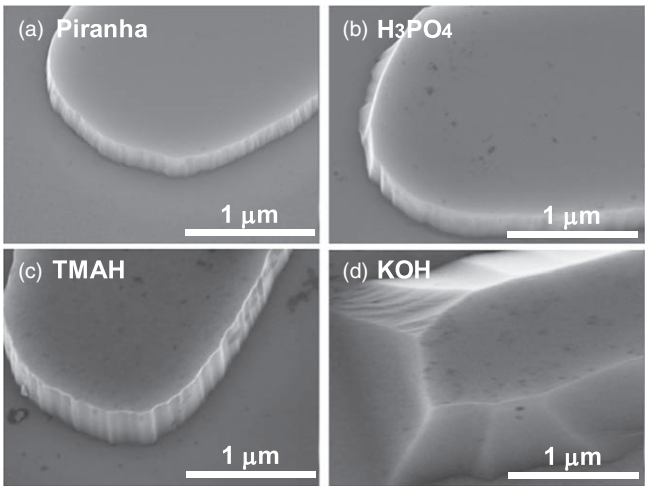

Fig. 3. Bird-view SEM image of β-Ga_2O_3 (010) dipped in (a) piranha solution at 120 °C for 30 min, (b) H_3PO_4 solution at 80 °C for 10 min, (c) TMAH solution at 80 °C for 30 min, and (d) KOH solution at 80 °C for 20 min.

effective etching, as shown in Fig. 3(d). The etch-rate difference between the TMAH and KOH solutions is attributed to the potassium ions, which have the large diffusion length in oxide layers,[19)] and a higher density of OH^- ions in the KOH solution than that of the TMAH solution. We suggest that Ga_2O_3 is dissolved in the base solutions after Ga–O compounds are formed by reacting Ga atoms with OH^- ions.[15,20)] Thus, the etching behavior in alkali solutions significantly depends on the crystal orientation, which defines the different Ga-to-O ratio, dangling bond densities, and surface energies. The strong Ga–O bonds in some crystal orientations including the (010) plane may suppress the reaction of Ga atoms with OH^- ions,[15)] resulting in chemically stable surfaces, or anisotropic etching.

The (010) orientation was used for the above dry and wet etchings of β-Ga_2O_3. Currently, β-Ga_2O_3 (010) epilayers are not commercially available. Using the (001) orientation, we investigated the effect of various chemical solutions on the vertical β-Ga_2O_3 SBDs with mesa termination. We used 10-μm-thick silicon-doped Ga_2O_3 films grown on 650-μm-thick tin-doped β-Ga_2O_3 (001) substrates by halide vapor-phase epitaxy. The substrates were thinned to ∼300 μm thickness from (00$\bar{1}$) backside by grinder, followed by CMP treatment with colloidal silica for 6 min at 50 rpm. After a 100-nm-thick nickel-metal mask was deposited on (001) surfaces by the EB evaporation, a 770-nm-deep mesa termination was fabricated by RIE at the ICP power of 300 W with the Cl_2/BCl_3 mixing gas of 10/10 sccm. The nickel metal was removed by the piranha solution in order to remove both plasma damages on the mesa surface and sidewall, which are potentially caused by the 300 W ICP power due to the large-size mesa patterns. Then, the samples were dipped in various chemical solutions at 80 °C for 10 min. For a cathode contact, Ti (20 nm)/Au (50 nm) metal stacks were deposited on the (00$\bar{1}$) backside, followed by a thermal annealing at 550 °C for 1 min in a nitrogen ambient. Circular anode contacts with various diameters of 100–500 μm were prepared on the (001) surfaces using Ni (20 nm)/Au (50 nm) metal stacks. The current density–voltage (J–V) and capacitance–voltage (C–V) characteristics of the β-Ga_2O_3 (001) SBDs with mesa

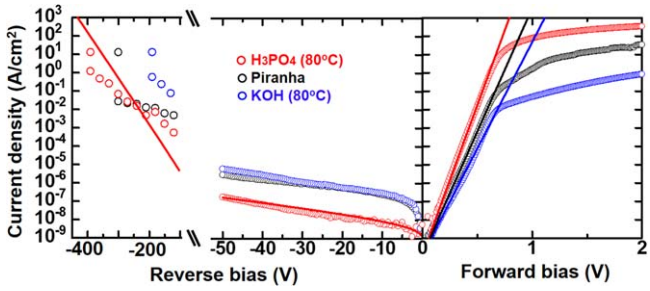

Fig. 4. (Color online) *J–V* characteristics of Ni/n-type β-Ga_2O_3 (001) SBDs with mesa termination dipped in hot-H_3PO_4, piranha, and hot-KOH solutions. The solid lines at forward and reverse biases are curves calculated using the TE and TFE models, respectively.

termination were performed using an Agilent B1505 semiconductor analyzer. The breakdown voltages of the Ga_2O_3 SBDs were determined in Fluorinert FC-72.

The *C–V* measurements of the Ga_2O_3 SBDs were performed at 1 MHz with a DC bias sweeping from −3 V to 0 V using 500-μm-diameter Ni contacts. The effective donor concentrations N_d–N_a and built-in potential V_d are determined from the equation of $\frac{1}{C^2} = \frac{2(V_d - V)}{A^2 e\varepsilon_s\varepsilon_0 (N_d - N_a)}$, where e is the electron charge, ε_s (∼10) is the relative permittivity of β-Ga_2O_3,[21] and A is the area of the anode electrode. N_d—N_a and V_d of the n-type Ga_2O_3 epilayer are calculated to be $2.5 \times 10^{16}\,cm^{-3}$ and 0.88 eV, respectively. The Schottky barrier height Φ_{B_CV} is determined from the equation of $e\Phi_B = eV_d + E_c - E_f + kT$, where k is the Boltzmann constant, T is the absolute temperature, and E_c and E_f are the bottom of the conduction band and the Fermi level in β-Ga_2O_3, respectively. By assuming silicon donors fully ionized at room temperature, E_c-E_f is equal to $kT \ln \frac{N_c}{N_d - N_a}$, where N_c $(=2\left(\frac{2\pi m_n kT}{h^2}\right)^{\frac{3}{2}})$ is the effective density of states in the conduction band. m_n (∼0.28m_0 for Ga_2O_3) is the density-of-state effective mass for electrons[22] and h is the Plank constant. By ignoring the image-force-induced lowering of the barrier height, Φ_{B_CV} of Ni for the Ga_2O_3 SBDs is calculated to be 1.03 eV. This value is slightly lower than those of the other reports $(1.2 \pm 0.2\,eV)$[4,23–26] and the ideal Schottky barrier height, which is estimated to be 1.2 eV by assuming electron affinities of 4.0 eV for UID β-Ga_2O_3 and a work function of 5.2 eV6 for Ni.[27] The low Φ_B may result from the lateral distribution of barrier inhomogeneity due to the large-sized electrode.[24,28]

The *J–V* characteristics of the β-Ga_2O_3 (001) SBDs treated by various chemical solutions are shown in Fig. 4. R_{on} of Ga_2O_3 SBDs treated by the H_3PO_4, piranha, and KOH solutions was 0.91, 41.0, and 850 mΩ-cm^2, respectively. The low R_{on} of the Ga_2O_3 SBDs treated by the H_3PO_4 solution is attributed to the substrate thinning, low ohmic-contact resistance, and low plasma damage. The maximum current density and on/off ratio was 340 A cm^{-2} at +2 V and ∼10^{10}, respectively. The forward bias *J–V* characteristics were analyzed using the thermionic emission (TE) model expressed as $J = J_0\left[\exp\left(\frac{eV}{nkT}\right) - 1\right]$, where J_0 $(=A^*T^2 \exp\left(-\frac{e\Phi_B}{kT}\right))$ is the saturation current density. The Schottky barrier height Φ_{B_JV} at the metal/semiconductor interface and the Richardson constant A^* $(=\frac{4\pi e m_n k^2}{h^3})$ are required to fit the exponential portion of the *J–V* characteristics. Using $A^* = 33.5\ Acm^{-2}K^{-2}$, Φ_{B_JV} for the Ga_2O_3 SBDs treated by the H_3PO_4, piranha, and KOH solutions are calculated to be 0.97, 0.99, and 1.00 eV, respectively, close to Φ_{B_CV}. n of the Ga_2O_3 SBDs treated by the H_3PO_4, piranha, and KOH solutions are 1.03, 1.21, and 1.35, respectively. The Ga_2O_3 SBDs treated by the H_3PO_4 solution have n close to unity, implying that the nearly ideal *J–V* characteristic is realized by removing the plasma damages. In these devices, we could not clarify the relation between the electrical properties and the plasma-damage area, i.e. the mesa top surface or sidewall. Further investigation using smaller-size electrodes is necessary.

For the reverse bias *J–V* characteristics, we use the thermionic field emission (TFE) model expressed as $J_{TFE} = \frac{A^*TE\hbar E}{k}\sqrt{\frac{\pi}{2m_nkT}}\exp\left[-\frac{1}{kT}\left(e\Phi_B - \frac{\alpha(e\hbar E)^2}{m_n(kT)^2}\right)\right]$,[29,30] where E is the electric field at the metal/semiconductor interface $(E = \sqrt{\frac{2e(N_d - N_a)(V_d - V)}{\varepsilon_s\varepsilon_0}})$. V_d and $N_d - N_a$ are obtained from *C–V* measurements, and Φ_B is obtained from the forward bias *J–V* measurements. The calculated curves using the TFE model are shown as a solid line at the reverse-bias side in Fig. 4. The TFE model is very close to the experimental data with the H_3PO_4 treatment, indicating that the reverse current is the intrinsic characteristics of the Ni/Ga_2O_3 Schottky contact. The SBDs treated by piranha and KOH solutions had the large leakage current, implying that the plasma damage remains. The current density of Ga_2O_3 SBDs increased with increasing reverse bias and reaches 1 A cm^{-2} at the reverse bias around 300 V, corresponding to the TFE model. We consider that the leakage current derived from the plasma damage, defects and surface charges[31] are negligibly small for β-Ga_2O_3 (001) SBDs treated by the H_3PO_4 solution. Further reduction of the reverse current density could be achieved using an anode electrode with larger Φ_B and a Ga_2O_3 epilayer with a lower donor concentration.[32]

To summarize this work, we investigated dry and wet etchings of β-Ga_2O_3 and fabricated vertical Schottky barrier diodes (SBDs) with mesa termination using an optimal etching condition. Using an inductively-coupled plasma reactive-ion etching with a nickel-hard mask, a β-Ga_2O_3 (010) mesa structure is obtained at an etch rate of 77 nm min^{-1} in BCl_3/Cl_2 mixture gas, showing a smooth sidewall. We compare various acid and alkali solutions to remove the plasma damage. By immersing the SBDs in hot phosphoric-acid solution, the differential on resistance and ideality factor of β-Ga_2O_3 (001) vertical SBDs with mesa termination is reduced to 0.91 mΩcm^2 and 1.03, respectively. Current density at the reverse bias is in good agreement with thermionic field emission model.

Acknowledgments This work was financially supported by Rohm CO., Ltd. and JSPS KAKENHI Grant No. 16H06424, and was carried out with Nano-Processing Facility in the national institute of Advanced Industrial Science and Technology (AIST-NPF) and open facility in the university of Tsukuba.

ORCID iDs Hironori Okumura https://orcid.org/0000-0002-5464-9169

1) M. Higashiwaki, K. Sasaki, A. Kuramata, T. Masui, and S. Yamakoshi, Appl. Phys. Lett. **100**, 013504 (2012).
2) A. Kuramata, K. Konishi, S. Watanabe, Y. Yamaoka, T. Masui, and S. Yamakoshi, Jpn. J. Appl. Phys. **55**, 1202A2 (2016).
3) K. Konishi, K. Goto, H. Murakami, Y. Kumagai, A. Kuramata, S. Yamakoshi, and M. Higashiwaki, Appl. Phys. Lett. **110**, 103506 (2017).
4) W. Li, Z. Hu, K. Nomoto, Z. Zhang, J. Hsu, Q. Thieu, K. Sasaki, A. Kuramata, D. Jena, and H. Xing, Appl. Phys. Lett. **113**, 202101 (2018).
5) Z. Hu, K. Nomoto, W. Li, N. Tanen, K. Sasaki, A. Kuramata, T. Nakamura, D. Jena, and H. Xing, IEEE Elec. Device Lett. **39**, 869 (2018).

6) J. Yang, Z. Sparks, F. Ren, S. J. Pearton, and M. Tadjer, J. Vac. Sci. Technol. B **36**, 061201 (2018).
7) J. E. Hogan, S. W. Kaun, E. Ahmadi, Y. Oshima, and J. S. Speck, Semicond. Sci. Technol. **31**, 065006 (2016).
8) L. Zhang, A. Verma, H. Xing, and D. Jena, Jpn. J. Appl. Phys. **56**, 030304 (2017).
9) Z. Jian, Y. Oshima, S. Wright, K. Owen, and E. Ahmadi, Semicond. Sci. Technol. **34**, 035006 (2019).
10) Z. Hu et al., Appl. Phys. Lett. **113**, 122103 (2018).
11) Y. Zhang, A. Mauze, F. Alema, A. Osinsky, and J. S. Speck, Appl. Phys. Exp. **12**, 044005 (2019).
12) S. Ohira and N. Arai, Physica Status Solidi C **5**, 3116 (2008).
13) T. Oshima, T. Okuno, N. Arai, Y. Kobayashi, and S. Fujita, Jpn. J. Appl. Phys. **48**, 040208 (2009).
14) Y. Zhang, A. Mauze, and J. S. Speck, Appl. Phys. Lett. **115**, 013501 (2019).
15) S. Jang, S. Jung, K. Beers, J. Yang, R. Ren, A. Kuramata, S. J. Pearton, and K. H. Baik, J. Alloy Compd. **731**, 118 (2018).
16) J. E. Hogan, S. W. Kaun, E. Ahmadi, Y. Oshima, and J. S. Speck, Semicon. Sci. Tech. **31**, 065006 (2016).
17) M. A. Lieberman and A. J. Lichtenberg, *Principles of Plasma Dischages and Materials Processing* (Wiley, New York, 2005).
18) A. P. Shah and A. Bhattacharya, J. Vac. Sci. Tech. A **35**, 041301 (2017).
19) O. Tabata, Sensors Mater. **13**, 271 (2001).
20) D. Li, M. Sumiya, S. Fuke, D. Yang, D. Que, Y. Suzuki, and Y. Fukuda, J. Appl. Phys. **90**, 4219 (2001).
21) M. Passlack, N. E. J. Hunt, E. F. Schubert, G. J. Zydzik, M. Hong, J. P. Mannaerts, R. L. Opila, and R. J. Fischer, Appl. Phys. Lett. **64**, 2715 (1994).
22) J. B. Varley, J. R. Weber, A. Janotti, and C. G. Van de Walle, Appl. Phys. Lett. **97**, 142106 (2010).
23) A. Jayawardena, A. C. Ahyi, and S. Dhar, Semicon. Sci. Tech. **31**, 115002 (2016).
24) T. Oshima, A. Hashiguchi, T. Moribayashi, K. Koshi, K. Sasaki, A. Kuramata, O. Ueda, T. Oishi, and M. Kasu, Jpn. J. Appl. Phys. **56**, 086501 (2017).
25) K. Sasaki, D. Wakimoto, W. T. Thieu, Y. Koishikawa, A. Kuramata, M. Higashiwaki, and S. Yamakoshi, IEEE Elect. Dev. Lett. **38**, 783 (2017).
26) K. Irmscher, Z. Galazka, M. Pietsch, R. Uecher, and R. Fornari, J. Appl. Phys. **110**, 063720 (2011).
27) M. Mohamad, K. Irmscher, C. Jannowitz, Z. Galazka, R. Manzke, and R. Fornari, Appl. Phys. Lett. **101**, 132106 (2012).
28) G. Jian et al., AIP Adv. **8**, 015316 (2018).
29) F. A. Padovan and R. Stratton, Solid State Electron **9**, 695 (1966).
30) T. Hatakeyama and T. Shinohe, Mater. Sci. Forum **389**, 1169 (2002).
31) R. Lingaparthi, K. Sasaki, Q. T. Thieu, A. Takatsuka, F. Otsuka, S. Yamakoshi, and A. Kuramata, Appl. Phys. Exp. **12**, 074008 (2018).
32) M. Higashiwaki et al., Appl. Phys. Lett. **108**, 133503 (2016).